



Contents lists available at ScienceDirect

Aerospace Science and Technology

www.elsevier.com/locate/aescite

1

2

3

4

5

6

7

8

9

10

11

12

13

14

15

16

17

18

19

20

21

22

23

24

 67
68
69
70
71
72
73
74
75
76
77
78
79
80
81
82
83
84
85
86
87
88
89
90
91
92
93
94
95
96
97
98
99
100
101
102
103
104
105
106
107
108
109
110
111
112
113
114
115
116
117
118
119
120
121
122
123
124
125
126
127
128
129
130
131
132

A simultaneous use of a leading-edge fillet and a non-axisymmetrically contoured endwall in a turbine stage

Özhan H. Turgut¹, Cengiz Camci²

¹ *Machinery and Heat Transfer Laboratory of Aerospace Engineering, The Pennsylvania State University, USA*

ARTICLE INFO

Article history:

Received 14 April 2021

Received in revised form 23 June 2021

Accepted 16 July 2021

Available online xxxx

Communicated by Kivanc Ekici

Keywords:

Leading-edge fillets

Non-axisymmetric endwall contouring

Axial flow turbine aerodynamics

Experimental aerodynamics

RANS computations

ABSTRACT

Secondary flow minimization is a crucial problem in a turbine passage. In the present paper, three different strategies are investigated to reduce the secondary-flow-related total pressure loss. These are leading-edge fillet, non-axisymmetric endwall contouring, and combining these two approaches. An experimental investigation in a single-stage turbine facility and RANS-based computations are performed to evaluate the designs. The experiments are carried out in the large-scale Axial Flow Turbine Research Facility AFTRF. A reference Flat Insert is installed on the nozzle guide vane passage's hub surface to allow future endwall design implementation during the experimental phase. The stereolithography manufactured reference insert has a constant thickness with a cylindrical shape. This investigation also uses four different leading-edge fillets, and they are attached to cylindrical Flat Insert initially. The same fillets are also attached to a contoured endwall. Simultaneous use of a leading-edge fillet and a non-axisymmetric contoured endwall for secondary flow control is the main objective of this research. Total pressure measurements are taken at the rotor inlet plane with a Kiel probe. The probe traversing is completed along one vane pitch and from 8% to 38% span. The leading-edge fillets effectively managed to weaken the horseshoe vortex occurring in front of the leading-edge. In one of the fillet cases sitting on the Flat Insert, the computational results at the NGV exit showed that the mass-averaged loss value was reduced by 1.31%. Three fillet designs decreased the area-averaged loss with a maximum reduction of 15.06%.

© 2021 Elsevier Masson SAS. All rights reserved.

1. Introduction

Sharma and Butler [1] states that the endwall losses represent 30–50% of the total pressure loss. Also, according to a very explanatory paper by Denton [2], 1/3 of the total loss in a turbine passage is governed by endwall losses. Two critical parameters play a significant role in producing endwall losses within and outside the turbine blade passage: the inlet boundary layer's thickness and the amount of turning of the blade. When the incoming boundary layer sees a blunt object, the fluid outside the boundary layer tends to turn onto low momentum fluid closer to the endwall. As a result, a roll-up vortex occurs in front of the leading edge, and this vortex separates into two parts, known as the horseshoe vortex. The strong cross-passage pressure gradient causes the pressure side leg of the horseshoe vortex to move towards the suction surface of the adjacent blade. This leg merges with the passage vortex,

and later on, the suction side leg wraps itself around this passage vortex. The strong crossflow within the blade passage, from the pressure side to the suction side, feeds this flow structure, enhances it, and lifts it off the endwall surface. It is clear from this secondary flow model that the horseshoe vortex's formation and the crossflow occurrence within the passage should be adequately treated.

Aerodynamic losses related to this horseshoe vortex can be minimized using a leading-edge fillet, filling the intersection of the nozzle guide vane (NGV) and the hub endwall. It forms a smooth transition from the NGV leading edge to the endwall surface. These leading-edge fillets are also advantageous from a heat transfer point of view. Minimizing the vortices results in lower mixing of the fluid near the midspan and near the endwall. Therefore, many researchers have been studying the effects of these leading-edge fillets on turbine NGV's. Sauer et al. [3] conducted one of the earliest studies using a leading-edge modification in turbine cascades. Their study aimed to reduce the secondary flow losses. The methodology was to design a bulb-like geometry at the leading edge endwall junction such that the suction side leg of the horseshoe vortex was strengthened. The interaction of this strong

¹ E-mail addresses: ozhan.turgut@prattwhitney.com (Ö.H. Turgut), cxc11@psu.edu (C. Camci).

² Presently, United Technologies Pratt & Whitney, CT, 06118, USA.

² Penn State University, 223 Hammond Bldg., University Park, PA 16802, USA.

<https://doi.org/10.1016/j.ast.2021.106985>

1270-9638/© 2021 Elsevier Masson SAS. All rights reserved.

1

2 Nomenclature

| | |
|-----------------|---|
| c | midspan axial chord length of the nozzle guide vane |
| AFTRF | Axial Flow Turbine Research Facility |
| c_{hub} | Midspan axial chord length of the nozzle guide vane |
| C_{pt} | Total pressure coefficient, $\frac{P_{02} - P_{01}}{0.5\rho V_1^2}$ |
| H | Height of the leading edge fillet |
| LE | Leading Edge |
| L_{up} | Length of the leading edge fillet measured from the leading edge in the upstream direction |
| L_{ss} | Length of the leading edge fillet measured from the leading edge along the suction surface |
| L_{ps} | Length of the leading edge fillet measured from the leading edge along the pressure surface |
| NGV | Nozzle Guide Vane |
| P_0 | Total pressure |
| $Re_{\theta t}$ | Momentum-thickness Reynolds number |
| Span | Spanwise distance measured from the hub normalized by NGV passage height |
| SLA | Stereolithography |

| | |
|----------|---|
| V | Velocity magnitude |
| x | Axial distance from nozzle guide vane leading edge |
| y^+ | Non-dimensional wall coordinate, $\frac{\sqrt{\tau_w/\rho} \cdot y_p}{v}$ |
| y_p | First grid height off the wall |
| γ | Intermittency |
| θ | Circumferential direction |
| ν | Kinematic viscosity |
| ρ | Density |
| τ_w | Wall shear stress |
| ω | Turbulent frequency |
| 1 | One axial chord upstream of nozzle guide vane leading edge |
| 2 | Nozzle guide vane exit plane, $\frac{x}{c} = 1.025$ |
| N | Turbine nozzle guide vane |
| R | Turbine rotor blade |
| rpm | Rotations per minute |
| SST | Shear stress transport |
| TKE | Turbulence kinetic energy |

suction side leg with the counterrotating pressure side leg (which merges with the passage vortex) would keep the passage vortex away from the profile boundary layer resulting in reduced endwall losses. They tested three different bulb-like geometries at the intersection of the leading edge and the endwall. Unlike a fillet, this bulb geometry was orthogonal to the endwall at the intersection line. Their results showed a 47% decrease in endwall loss, defined as the measured loss minus the inlet boundary layer loss and the profile loss. This level of the reduction came from a non-symmetric bulb geometry. Their computational results did not match the experimental results at a great rate.

Zess and Thole [4] conducted another leading-edge fillet experiment. They tried to eliminate the horseshoe vortex using a fillet with one boundary layer thickness in height and two boundary layer thickness in length. The most efficient fillet geometry was found after many CFD calculations, and then it was experimentally evaluated. The authors achieved to eliminate the horseshoe vortex and observed a reduction in the passage vortex. Results also showed a decrease in the level of streamwise vorticity and turbulent kinetic energy. However, the authors did not mention about the secondary loss measurements.

Shih and Lin [5] carried out computational studies to see the effects of the leading edge fillets and the given inlet swirl on the secondary flows, losses related to these secondary flows, and the surface heat transfer. Two different leading-edge fillets were tested. One had zero thickness on the blade surface, and the other had zero thickness on the endwall. The authors claimed that both inlet swirl and leading-edge fillets could reduce surface heat transfer (10% on the airfoil and 30% on the endwalls) and the aerodynamic losses by more than 40% on their own. The authors concluded that even though the horseshoe vortices and the crossflows were not eliminated, the losses and the heat transfer coefficient were reduced.

Lethander et al. [6] used an optimization program together with CFD software to design an effective leading-edge fillet to minimize the adiabatic wall temperature at the junction of the blade and the endwall. The results showed that the fillet hindered the formation of the horseshoe vortex, which in turn avoided the full development of the passage vortex. Nevertheless, total pressure loss increased slightly. Still, the fillet was able to perform well in terms of thermal benefits. The reduction in the secondary flows prevented the cooler near-wall fluid from lifting off from the endwall and the fillet surface.

Becz et al. [7] performed wind tunnel tests using Sauer et al.'s [3] two bulb-like geometries and a leading-edge fillet to compare them with the baseline configuration. The design of Sauer et al. [3] was used to create these bulbs. The fillet had two boundary layer thicknesses in height and eight boundary layer thicknesses in length. Area averaged total pressure loss results at a downstream location showed that the large bulb geometry slightly increased the loss. On the other hand, the small bulb and leading-edge fillet reduced the loss by 8%. In the later paper of Becz et al. [8], authors carried out experiments on the small bulb and leading-edge fillet. However, this time, they showed the mass-flow averaged total pressure loss results. The reason was to take into account the effect of mass flux to calculate the entropy production correctly. Compared to the first paper [7], the small bulb did not reduce total pressure loss. The leading edge fillet geometry again showed a reduction in the aerodynamic loss by 7.3%.

Mahmood et al. [9] experimented with leading-edge fillets on secondary flows and Nusselt Number in a linear turbine cascade. Four different types of fillets were tested, details of which are given in the paper. A smaller horseshoe vortex occurred in front of the leading edge based on flow visualizations compared to baseline. Their total pressure loss coefficient results, measured at a downstream location, exhibited no reduction. The authors also noted that the passage vortex shifted upwards. Hu et al. [10] numerically investigated the aerodynamic losses in a high-pressure turbine cascade with a contoured endwall under the influence of incoming wakes. The cascade's general aerodynamics did not improve in terms of energy loss characteristics with the increase of the passing frequency of incoming wakes. Kiran and Anish [11] studied non-axisymmetric endwall profiling's effects on a linear turbine cascade's aerodynamic performance at different incidence angles. The endwall profiling minimized the rolling up of the passage vortex and influenced the passage vortex to migrate closer to the endwall. This flow modification reduced the losses in the core flow but enhanced the losses near the endwall.

Han and Goldstein [12] performed mass transfer experiments in a turbine cascade with a leading-edge fillet. The leading edge fillet was designed similarly as described in [4] with modified dimensions. Their experiments included low and high turbulence intensity flow conditions at the inlet. The horseshoe vortex was reduced, and the passage vortex was delayed for both turbulence levels. However, the strength of the passage vortex was similar in magnitude to the baseline case near the trailing edge of the blade.

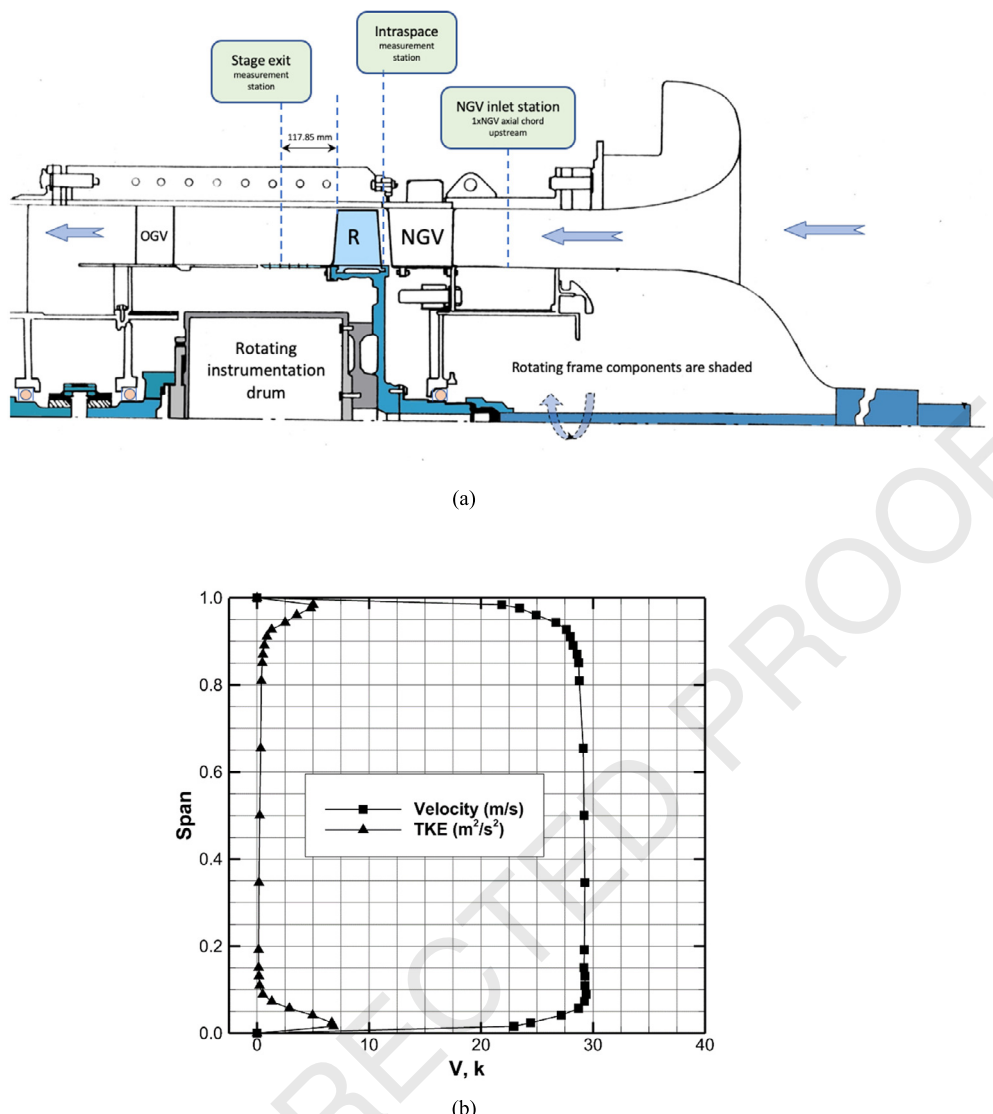


Fig. 1. (a) Turbine research facility AFTRF. (b) Measured inlet boundary conditions showing boundary layer and turbulent kinetic energy profiles, [20], [21], [22], and [23].

The authors also noted that the fillet increased the leading edge corner vortices on the suction and pressure sides. They did not mention about the total pressure losses.

The influence of leading-edge fillet shapes on the secondary flow field in a transonic axial flow turbine stage was computationally investigated by Ananthakrishnan and Govardhan [13]. The flow-field results showed a significant reduction in the total pressure losses associated with the horseshoe vortex near the leading edge region as the fillet radii are varied.

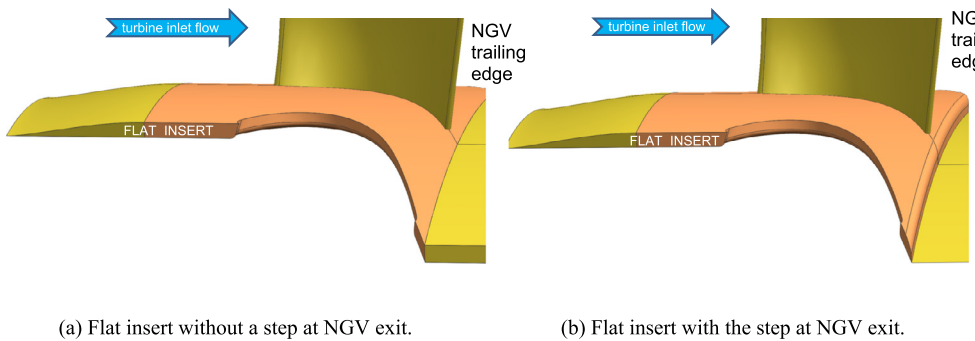
The current investigation includes the experimental investigation of the specific NGV leading edge fillets designed for the Axial Flow Turbine Research Facility (AFTRF). The aerodynamic performance of these fillets is experimentally tested on the cylindrical hub surface and a non-axisymmetric contoured endwall. Details of the specific non-axisymmetric contoured endwall design methodology were previously presented by Turgut and Camci in [14] and [25]. The current methodology benefitted from Fourier series-based splines at various axial locations on the hub surface. The individual splines were generated and combined with the help of streamwise B-splines within a solid modeling program. Using the first three terms of the Fourier series expansion, one can adequately define curves useful for non-axisymmetric endwall contouring purposes. The second step in non-axisymmetric contour

generation is to import the previously created endwall splines into a solid modeling program. The splines, already defined in MATLAB at different axial locations, are transferred by the program. Next, the solid modeling program creates a contoured surface with the help of B-Splines to combine these imported splines. Other design methods for endwall surfaces using non-axisymmetric contouring in the literature can be found in [15], [16], [17], [18], and [19].

This study focuses on the simultaneous use of the leading edge fillets combined with custom-designed non-axisymmetric endwall contouring based NGV hub surfaces. The following sections will give detailed information about the design methodology of these leading-edge fillets. The computational fluid dynamics evaluation also supports the aerodynamic experiments performed in this study, and the predictions are presented at the NGV exit.

2. Experimental facility

Turbine facility: The Axial Flow Turbine Research Facility AFTRF is a single-stage, cold-flow turbine with a diameter of 91.66 cm. The (AFTRF) is operational at the Turbomachinery Aero-Heat Transfer Laboratory of the Pennsylvania State University, as shown in Fig. 1.a. The single-stage turbine consists of 23 NGV's and 29 rotor blades followed by the exit guide vanes that bring the rotor exit



(a) Flat insert without a step at NGV exit.

(b) Flat insert with the step at NGV exit.

Fig. 2. Backward facing step at NGV exit.**Table 1**
The AFTRF design performance parameters.

| | |
|--|--------|
| Inlet total temperature (°K); T_{01} | 289 |
| Inlet total pressure (kPa); P_{01} | 101.36 |
| Mass flow rate (kg/s); Q | 11.05 |
| Rotational speed (rpm); N | 1300 |
| Total pressure ratio; P_{01}/P_{03} | 1.0778 |
| Total temperature ratio; T_{03}/T_{01} | 0.981 |
| Pressure drop (mmHg); $P_{01} - P_{03}$ | 56.04 |
| Power (kW); P | 60.6 |

Table 2
The AFTRF geometrical design features.

| | |
|--|-------------------------|
| Rotor hub tip ratio | 0.7269 |
| Tip radius (m); R_{tip} | 0.4582 |
| Blade height (m); h | 0.1229 |
| Tip relative Mach number | 0.24 (max) |
| Nozzle guide vane (tip) number | 23 |
| chord (m) | 0.1768 |
| spacing (m) | 0.1308 |
| turning angle | 70 |
| maximum thickness (mm) | 38.81 |
| Midspan axial chord nozzle (m) | 0.1123 |
| rotor (m) | 0.09294 |
| Vane Reynolds number based on inlet velocity | $(3\sim4) \times 10^5$ |
| based on exit velocity | $(9\sim10) \times 10^5$ |

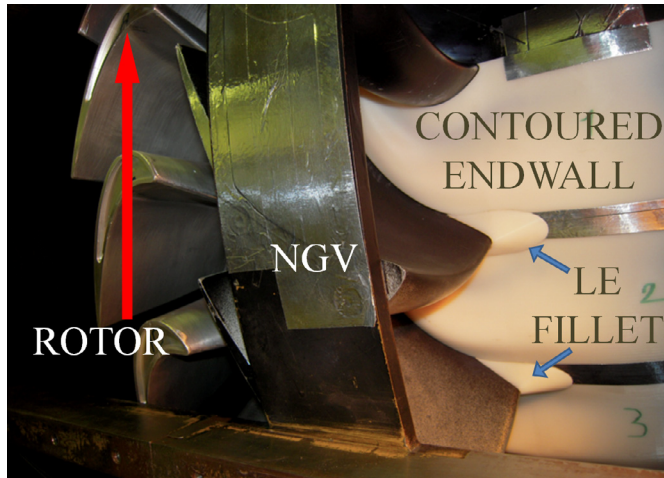
flow into the axial direction just before the suction blowers. Inlet has a bell-mouth shape followed by the NGV row and the rotor blades. The AFTRF inlet bell-mouth section is at atmospheric pressure. A set of four axial suction blowers located downstream of the rotor provides the pressure drop necessary for the rotor's steady operation. A power-absorbing eddy-current brake controls the rotational speed of the rotor within ± 1 rpm. The measured stage inlet velocity and turbulent kinetic energy profile in the spanwise direction are shown in Fig. 1.b. The two profiles belong to an axial location, one chord length upstream of the NGV airfoil at the mid-span. Table 1 summarizes the turbine facility's design performance parameters, and the pertinent geometrical features are listed in Table 2. The references [20], [21], [22], and [23] include a detailed description and the characteristics of the AFTRF.

Definition of the flat insert and the rationale for the insert: Implementing highly three-dimensional and non-axisymmetric hub endwall surfaces is convenient by allocating a cylindrical flat insert volume, as shown in Fig. 2. The flat insert has a sharp wedge-shaped inlet ramp for a smooth transition from the facility's original hub surface to the new experimental hub surface. The perfectly cylindrical flat insert volume, as shown in Fig. 2, eventually

houses the new non-axisymmetric endwall contoured hub surface under investigation. This approach makes installing any new non-axisymmetric hub design into the turbine research rig very convenient with high time and cost savings. The *Flat Insert* is manufactured using the stereolithography (SLA) technique to assess the performance of the contoured endwall and the leading edge fillet designs against a reference baseline. This *Flat Insert* has a cylindrical endwall surface as the inner hub surface of the NGV passage and has a thickness of 0.0075 m, corresponding to $\sim 6.1\%$ of the vane span. It extends one midspan axial chord of the vane in the upstream direction. It has a linear ramp with rounded edges to maintain surface continuity. The *Flat Insert* ends at the rim seal with a backward-facing step. The solid model of this insert is shown in Fig. 2. The effect of this backward-facing step will be investigated computationally in the following sections.

Installation of the endwall designs and fillets: Fig. 3 illustrates a simultaneous installation of a non-axisymmetric contoured endwall and a fillet on the NGV inner hub surface of AFTRF. A comprehensive description of the non-axisymmetric contoured endwall design methodology was previously published by the authors in [11] and [22]. Fig. 3 also shows a view of the NGV row and the SLA parts from the upstream of the leading edge. Note that 0.05 mm (2 mils) thin aluminum tape is used for the continuity between the surfaces. SLA parts are attached to the hub surface with double-sided tape. The blue vertical line in Fig. 4 indicates the experimental measurement plane. This axial plane is located at $x/c = 1.018$ from the NGV trailing edge at the casing. The radial starting location for the measurements is selected as 8% of the vane span. The reason for this selection is that the thicknesses of SLA parts downstream of the trailing edge are 6.1% of the vane span. It is also observed that above 35% of the NGV span, the variations in measurements due to fillet or endwall modifications are minimal. Therefore, the maximum sampling location in the radial direction is selected as 38% of the span. This selection helped reduce the time needed for complete local measurement along one NGV pitch in the circumferential direction.

Total pressure measurements at NGV exit: The total pressure measurements are carried out by a Kiel probe manufactured by United Sensor Corporation [24]. The probe has a 3.175 mm (0.125in.) head diameter. The main advantage of Kiel probe is the extensive range of insensitivity to yaw and pitch angles. The manufacturer documents the ranges as $\pm 48^\circ$ and $\pm 45^\circ$ for yaw and pitch, respectively. Before the experiments, the probe is manually aligned with the NGV exit flow design angle, which is 70° from the axial direction. Zaccaria and Lakshminarayana [20] reported that the flow yaw and pitch angles deviate from the design value within $\pm 5^\circ$. The probe is mounted on a single-axis linear traverser, which moves in the radial direction. This linear traverser is installed on a circumferential traverser that is attached to the facility window. The slot on the window allows the circumferential traversing mechanism to complete a 1.5 vane pitch. The probe



(a)



(b)

Fig. 3. Contoured endwall and fillet installation. (a) SLA manufactured contoured endwalls (white) attached to the inner hub surface. (b) Leading-edge fillets and the contoured endwall installation.

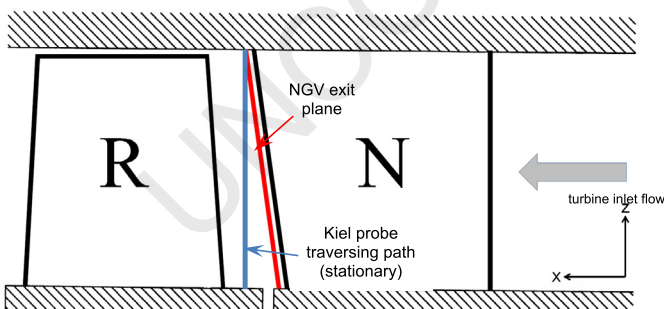


Fig. 4. Rotor inlet plane (Kiel probe traversing path) perpendicular to the axial direction and NGV exit plane parallel to NGV trailing edge. (For interpretation of the colors in the figure(s), the reader is referred to the web version of this article.)



traversing slot's axial position on the turbine casing is $x/c = 1.018$ near the NGV trailing edge at the casing. Nevertheless, the authors decided to traverse one full pitch in the circumferential direction for time-saving considerations. There are 18 radial and 25 circumferential locations where the probe collects 450 data points.

The measurement uncertainty: The Kiel probe is connected to a pressure transducer, and the analog data from the transducer is transferred to a 12-bit data acquisition (DAQ) board. A computer program is developed using the graphical interface software LabView, which reads the data coming from the DAQ. The program also performs the necessary post-processing and exports the total pressure coefficients C_{pt} values. The estimated uncertainty in measured C_{pt} is 0.6%.

3. Design methodology

Nonaxisymmetric endwall contouring: Non-axisymmetric endwall contouring is accomplished in two steps. The first step is to define splines within the vane passage at various axial locations. These splines are described in the form of Fourier series expansions. The first three terms of the Fourier series are sufficient to create highly complex circumferential curvature. Secondly, these splines are imported into the solid modeling software, in which they are combined to form a three-dimensional contoured endwall. A detailed description of the specific non-axisymmetric endwall contouring design method is given in the previous papers of Turgut and Camci [14] and [25]. In these two papers, analytical details of the contoured endwall generation were presented and computationally evaluated. Note that the throat area variation was around 1% of the total area, resulting in the same mass flow rate within the passage. Among all of the designs, case D14 was found to be promising. So that, it was tested experimentally to see its influence on the NGV exit total pressure distribution. Two recent non-axisymmetric endwall design methods, including the effects of purge flow and varying endwall contour geometry, are provided in [26] and [27].

Leading-edge fillet design: The horseshoe vortex formation mechanism and its bifurcation into two parts are not the same for all turbine blades. According to Langston [28], the separation at the saddle point where the horseshoe vortex stagnates on the endwall surface depends on the blade surface pressure distribution rather than the leading edge shape. A particular leading-edge fillet should be designed for each turbine blade type depending on the airfoil's loading characteristics. However, there are certain conventions to consider while designing the fillet. Sung and Lin [29] suggested designing the fillet such that its length is greater than its height in the spanwise direction. Also, they proposed the height to be at least one boundary layer thickness for symmetric airfoils. Zess and Thole [4] tried various configurations of height to length ratio. They also examined the fillet profile and decided on using a fillet with a linear slope.

ATRF implementation of the current fillet designs: Fig. 5 describes the LE fillet design parameters. H represents the fillet's height in the radial direction from the cylindrical endwall based on the vane span. L_{up} is the distance from the leading edge, showing how the fillet is extended in the upstream axial direction. L_{ps} and L_{ss} indicate the specific fillet's final boundaries on the pressure and suction surfaces, respectively. In the present study, four different types of LE fillets are introduced. Two of them have a linear cross-section, and the other two have parabolic cross-sections. The linear ones are named *F02linear*, *F03linear*, and the ones with parabolic profiles are called *F03curved*, *F04curved*. These four LE fillets are designed so that they are mounted directly on a cylindrical endwall. Moreover, the performance of these fillets is also investigated on the contoured endwall, namely *FC02linear*, *FC03linear*, *FC03curved*, *FC04curved*. *FC* stands for *Fillet and Contour*. Table 3 lists the design parameters for all these designs. In addition to this, Fig. 6 illustrates the solid model representation of the LE fillets. In this figure, the Flat Insert and the LE fillets sitting on cylindrical endwall are in the left two columns; the contoured endwall and the LE fillets designed for contoured endwall are in the right two

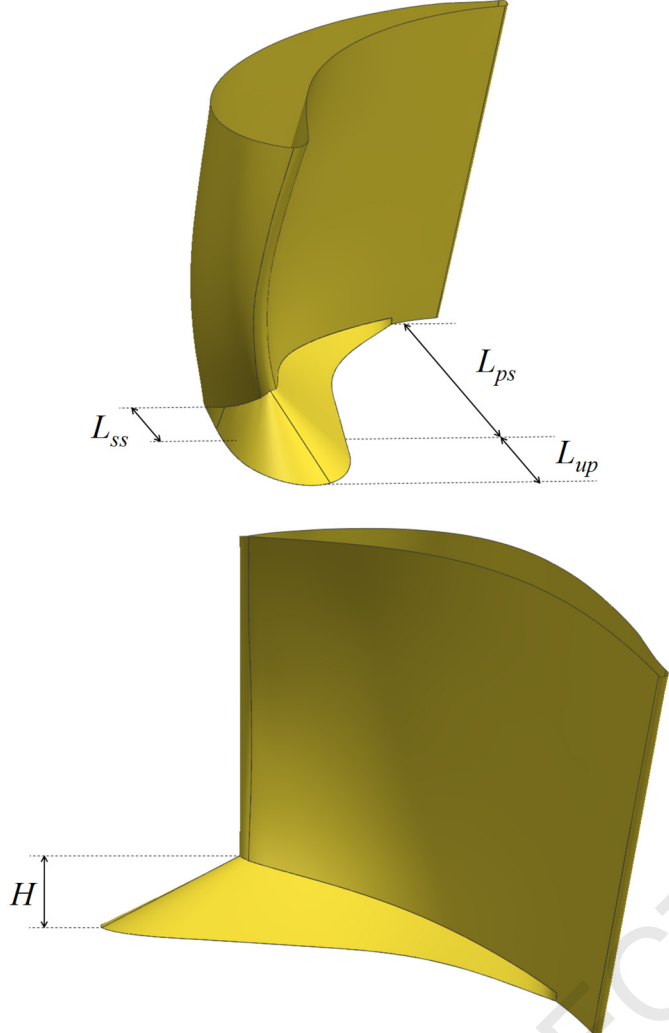


Fig. 5. The characteristic length definitions of the leading-edge fillet designs.

Table 3
Leading-edge fillet design features.

| | H % Span | L _{up} % c _{hub} | L _{ps} % c _{hub} | L _{ss} % c _{hub} |
|------------|-------------|---------------------------------------|---------------------------------------|---------------------------------------|
| F02linear | 0.08 | 0.27 | 0.28 | 0.22 |
| F03curved | 0.15 | 0.37 | 0.88 | 0.33 |
| F03linear | 0.15 | 0.37 | 0.88 | 0.33 |
| F04curved | 0.15 | 0.37 | 0.98 | 0.33 |
| FC02linear | 0.08 | 0.27 | 0.28 | 0.22 |
| FC03curved | 0.15 | 0.37 | 0.88 | 0.33 |
| FC03linear | 0.15 | 0.37 | 0.88 | 0.33 |
| FC04curved | 0.15 | 0.37 | 0.98 | 0.33 |

columns. F02linear and FC02linear have a design such that L_{up} is approximately twice the length as H . The remaining LE fillets have more aggressive designs, doubling the fillet's height and extending on the pressure side and hub intersection. F03 designs elongate on the pressure side as far as $c_{hub} = 0.88$, whereas F04 designs reach the $c_{hub} = 0.98$ point with more filling effect on the pressure side and hub intersection corner.

4. Computational details

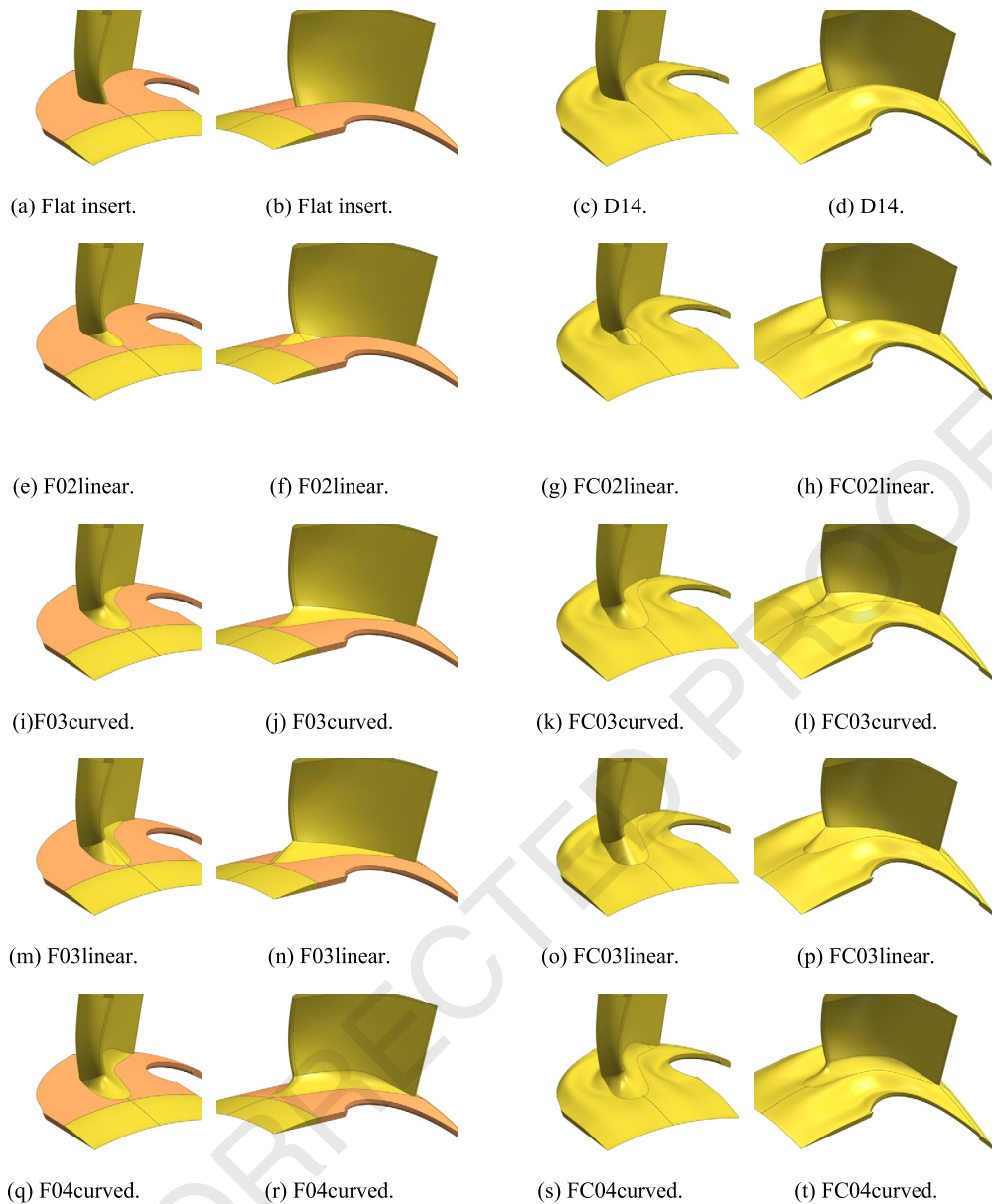
The finite volume method: The computational evaluations of the non-axisymmetric endwalls and leading-edge fillets are accomplished by the general-purpose finite-volume-based flow solver

ANSYS CFX. The steady-state, three-dimensional flow simulations are performed for an annular NGV passage without including the rotor section. The computational domain extends one axial chord (mid-span) in the upstream direction, where the experimental inflow conditions are imposed. The circumferentially averaged total pressure and turbulence kinetic energy distribution along the span are specified at the inlet boundary according to the previous experimental research in AFTRF [23]. The outflow boundary is located two chords downstream of the NGV trailing edge, and the mass flow rate is set at the outlet. NGV, hub, and casing walls have no-slip boundaries with adiabatic conditions. Only one NGV passage is simulated with circumferentially periodic sidewalls.

Turbulence model and Structured Grid Analysis With Transitional Flow Modeling: Menter's [30] two-equation eddy-viscosity model gives good predictions, especially when there is an adverse pressure gradient in the boundary layer. This Shear Stress Transport (SST) model is based on the $k-\omega$ turbulence closure formulation. Also, the flow through an NGV passage is transitional, and one should account for the transitional effects as discussed in [31,32]. A grid independence study is performed with different resolutions of the structured grid. As noted previously, it may be beneficial to use a multiblock-grid strategy for complex geometries to create a mesh almost orthogonal to the boundaries.

The first results with a structured grid are obtained with a fully turbulent flow assumption starting from the inlet of the computational domain. Transitional flow influence is not taken into account initially. Four different structured mesh sizes are compared, namely, 0.6, 1.0, 2.0, and 4.3×10^6 cells. The circumferentially mass-averaged total pressure coefficient distribution at the NGV exit shows that the profile losses of the NGV are not accurately predicted. For the 2.0 and 4.3×10^6 cell grids, the typical deviation is around 50%, and for 0.6 and 1.0×10^6 cell grids, it is about 100% when computations are compared to AFTRF experiments. These deviations appear to be very large, but note that the C_{pt} value at the midspan is approximately -0.05. As for the grid independence, it is clear from the figure that 2.0 and 4.3×10^6 cells give similar results.

The transitional flow over an uncooled turbine NGV or blade can be a genuine concern throughout CFD calculations. It is accepted that transition is mainly dominated by freestream turbulence level, x-Reynolds number, pressure gradient, type of surface curvature, and unsteady wake passing in turbine stages. The influence of heat transfer, surface curvature, surface roughness, and compressibility on transition is not as contributing as that of freestream turbulence level. Denton [2] argued that an inaccurate specification of the transition point, instead of predicting it within the calculation, may lead to weak quantification of turbine aerodynamic flows and heat transfer. Many researchers in the past tried to predict transition within two-equation turbulence models. Another approach is to employ empirical correlations as transition models. The Gamma-Re-Theta model selected to include transitional flow effects in the current computations uses two extra transport equations, one for the intermittency and the other for momentum thickness Reynolds number. The SST turbulence model with this correlation is already validated for various transitional flow cases [32]. The same type of multi-block structured grid discussed in the previous paragraphs is used to observe the transitional effects throughout the computations. The circumferentially averaged total pressure coefficient distribution in the spanwise direction at NGV exit was obtained for 0.6, 1.0, 2.0, and 4.3×10^6 computational cells. The grids with 2.0 and 4.3×10^6 cells predicted C_{pt} very close to experimental data along the wake and in the secondary flow zone near the hub. For computational time consumption considerations and the effective usage of computer resources, the authors selected the 2.0×10^6 cell grid structure

**Fig. 6.** Leading-edge fillet designs.

as a sufficient mesh resolution for adequately resolving the flow physics [32].

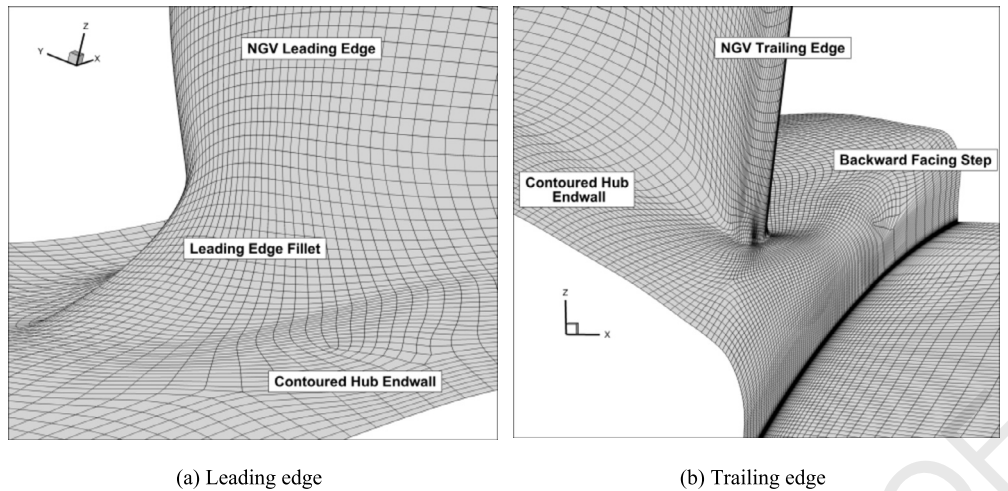
Fig. 7 shows an example of a generated structured grid. This figure shows the leading edge and trailing edge view of the FC04curved design. The structured grid is well adapted to the endwall contouring, leading-edge fillet, and backward-facing step. Since the near-wall grid resolution is the key for transitional flows and capturing the secondary flow formation, the non-dimensional wall distance of $y^+ < 1$ is satisfied everywhere in the domain. A total number of 2 million three-dimensional mesh elements are used in the computational domain. This mesh density reduces the grid dependency of the results considerably, especially on the total pressure coefficient distribution at the NGV exit.

Measurement planes for the assessments: The computational evaluation of the current designs is performed on two selected planes. One is the rotor inlet plane, where the experimental measurements are taken. This plane is normal to the axis of rotation. The other plane is parallel to the NGV trailing edge, located at $x/c = 1.025$ away from the trailing edge line, as shown in Fig. 4. The reason to have different comparative planes is to isolate the

effects of the backward-facing step existing at the exit of the NGV. The rotor inlet plane measurements include the influence of the backward-facing step located just downstream of the NGV trailing edge.

5. Results and discussion

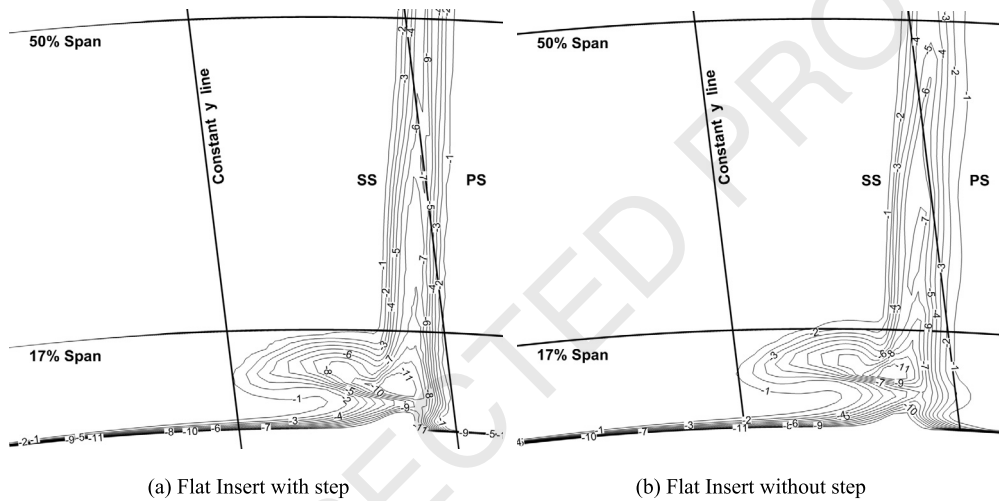
Flat Insert as a reference endwall: As mentioned in the previous sections, a Flat Insert is utilized as a reference endwall to evaluate new designs. The Flat Insert extends up to the end of the NGV row, and it has a backward-facing step shown in Fig. 2.b. This insert had to be fabricated that way because of the physical limitations of the facility. However still, it is essential to analyze the fluid flow structures behind this backward-facing step. A new solid model of Flat Insert is completed to isolate the step's flow effects without having a step, as shown in Fig. 2.a. This model is designed for computational assessment. After the NGV trailing edge, the cylindrical endwall extends to the domain's outflow boundary, which lies two c downstream.



(a) Leading edge

(b) Trailing edge

Fig. 7. Multi-block structured grid.

Fig. 8. Contours of C_{pt} at NGV exit plane, computational results.

The backward-facing step's flow impact: This flow influence is investigated both at the NGV exit plane and the rotor inlet plane. Contours of C_{pt} at the NGV exit plane tell that the main difference between these two cases is the secondary flow core location, as shown in Fig. 8. For the Flat Insert with step case, the core is closer to the endwall. The reason is that the radial velocity component of the flow near the endwall increases after the step, and hence, there occurs a downward motion of the flow in the radial direction. The downward tendency of the flow influences the upstream also, and the secondary flow region is pulled towards the hub endwall.

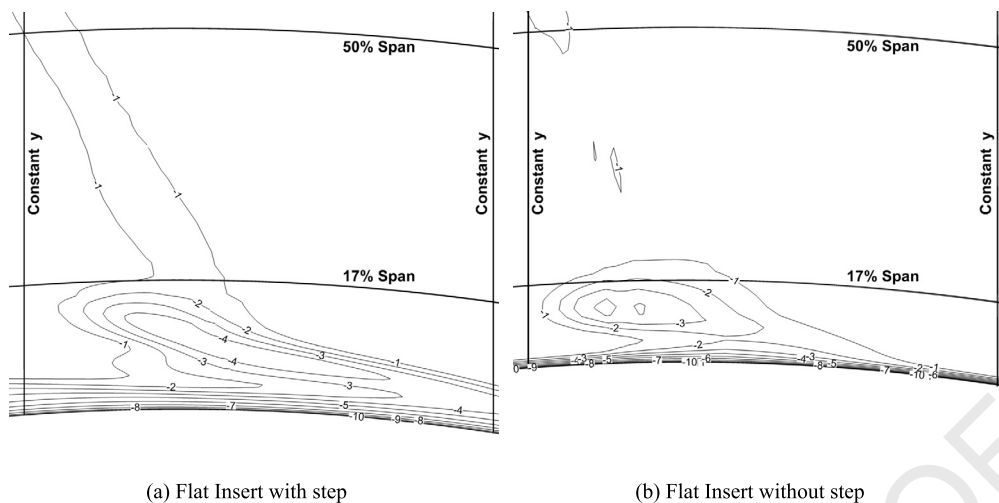
Fig. 9 shows the C_{pt} contours at the rotor inlet plane after the backward-facing step. It should be pointed out that the reference constant y lines in Fig. 9 are not the same as those in Fig. 8. Also, as a reminder, the hub endwall for Flat Insert without step starts around 6% span. It is clear from this figure that the upper edge of the secondary flow area remains almost at the same radial position for both cases. Another important observation is the minimum value of C_{pt} decreases to -4 for both cases. The contour plot for Flat Insert with step reveals that the secondary flow area is diffused towards the endwall after the step. On the other hand, Flat Insert without step has the secondary flow area more concentrated at a region. The wake is spread out for the case without step.

The circumferentially mass averaged C_{pt} distributions along the span for the NGV exit plane and rotor inlet plane are shown in Figs. 10.a and 10.b. As discussed previously, there is a radially out-

ward shift of approximately 1% span in the C_{pt} distribution at the NGV exit plane. The comparison in Fig. 10.a shows that the distributions do not change after 25% span with or without step.

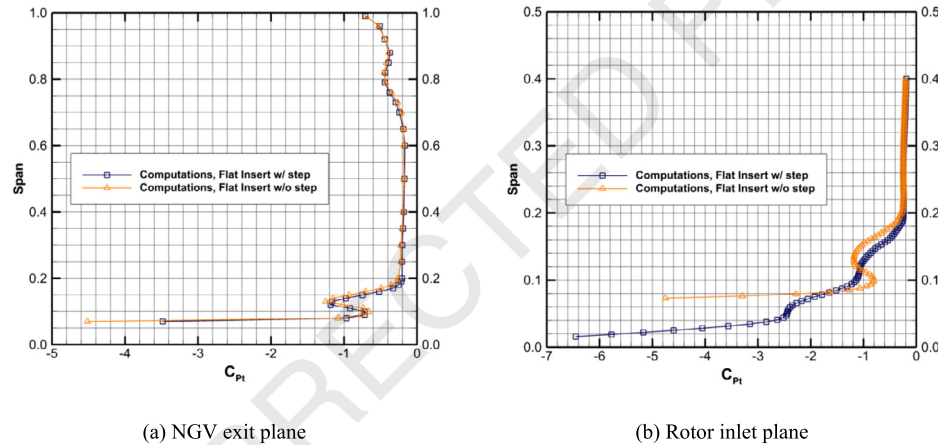
The observation downstream of the step shows that the case without step has a secondary flow more elevated in the spanwise direction, which is in accordance with Fig. 10.b. On the other hand, there are two kinks in the C_{pt} distribution of the case with a backward-facing step, as shown in Fig. 10.b. One is around 12% span, and the other one is near 6% span. The first one is related to the secondary flow, and it is closer to the endwall by 1% span than the Flat Insert without step. This result is similar to Fig. 10.a. The second kink occurs since there is a diffusion of the secondary flow after the step. It should be pointed out that the computation of recirculation and flow reattachment patterns behind backward-facing steps are dependent on the type of turbulence model and the near-wall treatment. A thorough discussion of these dependencies can be found in Kim et al. [33].

Effect of leading Edge Fillet: The purpose of using LE fillets is to minimize the vorticity content resulting from the horseshoe vortex formation. Fig. 11 depicts the LE fillet's functionality in reducing the strength of the horseshoe vortex. The Flat Insert endwall and LE junction are shown in Fig. 11.a. A circumferential plane, extending from the leading edge in the upstream direction, is extracted, and the streamlines are released on this plane. The horseshoe vortex is captured within the 5% of vane span, and it is magnified



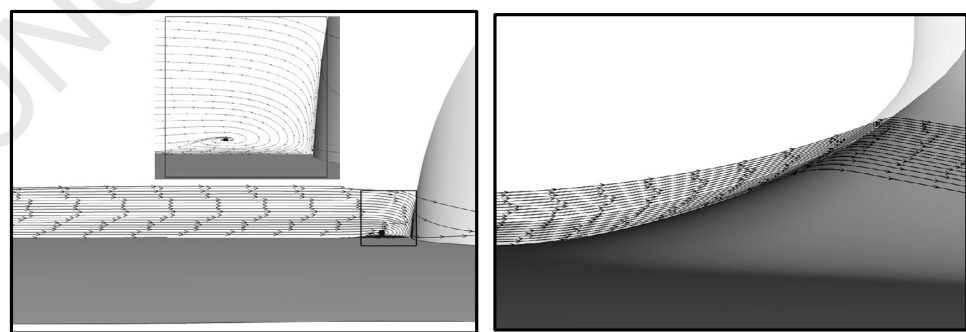
(a) Flat Insert with step

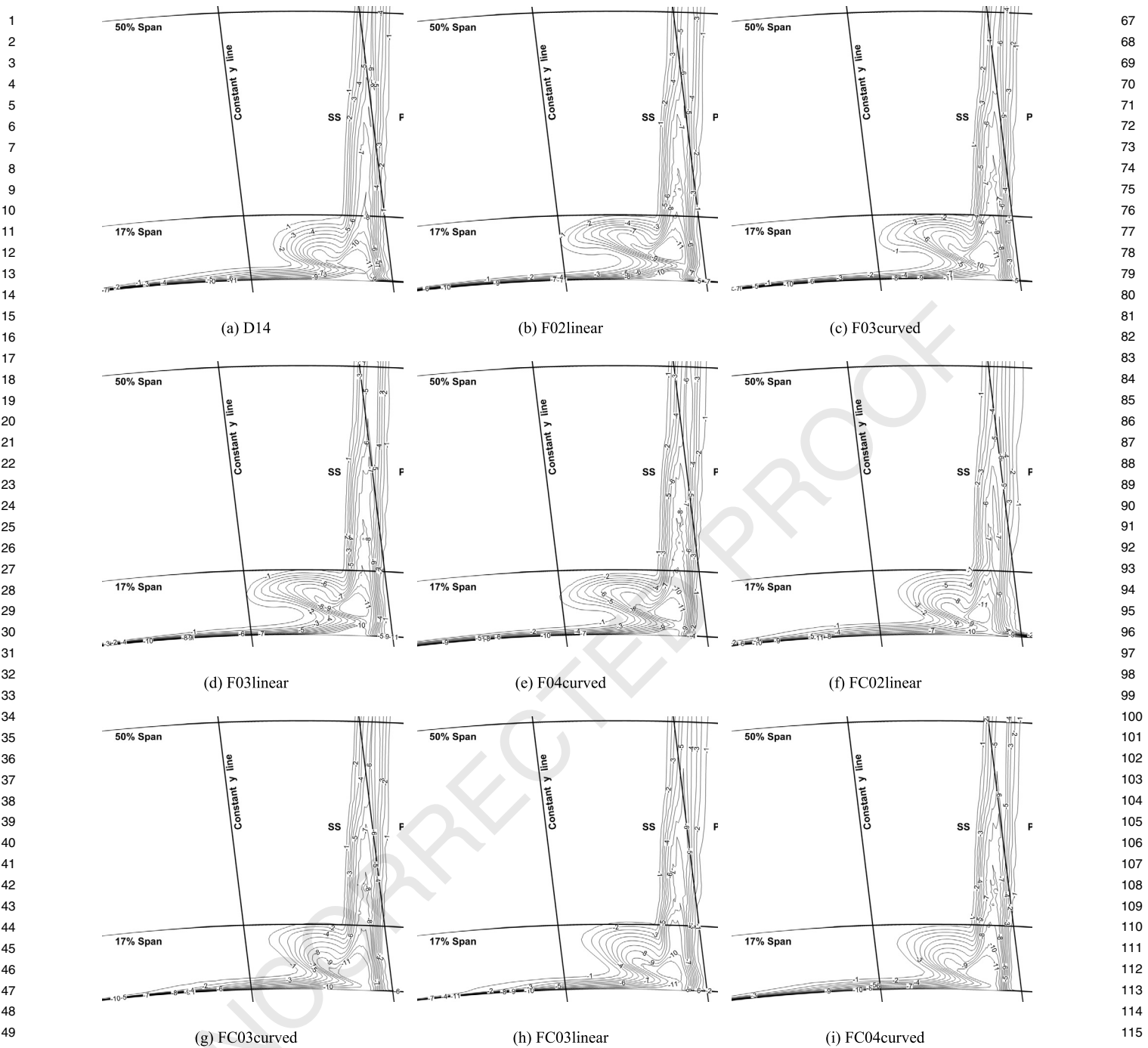
(b) Flat Insert without step

Fig. 9. Contours of $C_{p\theta}$ at rotor inlet plane, computational results.

(a) NGV exit plane

(b) Rotor inlet plane

Fig. 10. Effect of backward-facing step on $C_{p\theta}$, circumferentially averaged computational results.(a) Flat insert and endwall
and a regular NGV leading edge with
strong horseshoe vortex(b) The horseshoe vortex is nearly eliminated
with LE fillet**Fig. 11.** Effect of leading-edge fillet on horseshoe vortex formation.

Fig. 12. Computational C_{pt} contours at NGV exit plane.

for a better resolution. This horseshoe vortex is nearly eliminated with the LE fillet's utilization, as shown in Fig. 11.b. For both figures, the circumferential planes and the streamlines are the same. Since the flow does not meet the leading edge with a sharp corner at the hub, streamlines climb up the ramp and nicely follow the fillet geometry. Further details of the results with LE fillets will be examined at the NGV exit plane and rotor inlet plane in the following sections.

Contoured endwall and Leading Edge Fillet Designs: Four different LE fillet designs are evaluated both computationally and experimentally. These fillets are attached to the Flat Insert as well as the contoured endwall. The aim is to see the fillets' individual behavior on a cylindrical endwall surface and also analyze the per-

formance of these fillet designs in combination with the contoured endwall. As discussed earlier, there are two comparison planes, namely the NGV exit plane and the rotor inlet plane.

NGV exit plane computational results: Fig. 12 shows iso-contour lines of C_{pt} at the NGV exit plane. The same constant y lines in Fig. 8 are used to form a basis for comparison. The first thing that is apparent is the contoured endwall itself, and the combination of LE fillets with contoured endwall results in a smaller secondary flow area.

Contrary to this favorable result, contouring the endwall increases the total pressure loss just above the endwall. For instance, at a constant y location, the thickness of the total pressure loss contours reach up to 8.3% of the span for contoured endwall case

1 D14, as shown in Fig. 12.a. Whereas, for F03linear in Fig. 12.d, the
 2 thickness of the contour lines at the same y location is around
 3 7.5% span.

4 A more quantitative discussion can be achieved from the cir-
 5 cumferential mass flow averaged values. Fig. 13 shows the com-
 6 parison between the reference Flat Insert case and contoured endwall
 7 and LE fillet cases at the NGV exit plane. The sole effect of the con-
 8 toured endwall case, D14, is revealed in Fig. 13.a. Case D14 changes
 9 the C_{pt} distribution considerably. From 12% to 18% span, the cir-
 10 cumferentially mass flow averaged values are reduced compared
 11 to the Flat Insert case. The reduction reaches 33% of C_{pt} at 13%
 12 span. Conversely, from 11% span to the endwall, the total pressure
 13 loss is increased. This increase is mainly because the valley on the
 14 endwall near the suction surface pulls the secondary flow loss re-
 15 gion to the hub endwall. That results in higher values of C_{pt} near
 16 the endwall.

17 Fig. 13.b shows that F02linear reduced the mass averaged val-
 18 ues from 10% to 13% span but increased from 14% to 17%. There is
 19 a slight radially outward shift in the distribution, approximately
 20 0.5% span. The combination of contoured endwall and LE fillet,
 21 FC02linear, has a similar trend close to D14. From 16% to 12% span,
 22 C_{pt} is less than those of Flat Insert, and the maximum reduction is
 23 around 30% of C_{pt} .

24 F03curved reduced total pressure loss between 11% to 13%
 25 span, having a maximum reduction of 17% C_{pt} value, as shown in
 26 Fig. 13.c. FC03curved improved the loss distribution just above the
 27 endwall, 6.5% span compared to D14 in Fig. 13.a.

28 FC03linear in Fig. 13.d has a very similar distribution to that of
 29 FC03curved. The total pressure loss is decreased between 11%
 30 and 16%, with a maximum reduction of 33% C_{pt} . Moreover, it is
 31 increased between 11% and 8% span. Again, the fillet attached to
 32 the contoured endwall works effectively close to the hub endwall.
 33 It is seen from this figure that F03curved has shifted the profile
 34 0.6% span in the radially outward direction, between 11% and 18%
 35 span locations.

36 F04curved is the design extending on the pressure surface to
 37 the trailing edge corner. It covers a larger area at the intersection
 38 of the pressure surface and hub endwall. It decreased the peak
 39 value of C_{pt} by 12% around 12% span. However, the loss is in-
 40 creased by 34%, very close to the hub endwall. FC04curved has
 41 a similar distribution to that of FC03curved.

42 **Experiments at the rotor inlet plane and computations:** The
 43 authors of this paper performed the experiments at the rotor in-
 44 let plane. Fig. 14 presents the area-averaged total pressure coeffi-
 45 cient distributions. The solid lines represent the experimental data,
 46 whereas the dashed lines display computational simulation results.
 47 Before going into a detailed discussion of these figures, it is help-
 48 ful to mention one observation. The agreement between the ex-
 49 perimental and computational distribution, particularly below 23%
 50 span, is not very good. The wake C_{pt} values are predicted well, but
 51 the discrepancy starts at the secondary flow area. The deviation of
 52 the CFD simulation from the measurement has two main reasons:
 53

- 54 • Rotor-vane interaction is not included in the current simula-
 55 tion. The computations are carried on without the rotor. Only
 56 the NGV passage flow is simulated.
- 57 • There is a radially outward complex flow through the rim seal
 58 entering into the rotating blade passages. The CFD calculation
 59 does not involve this highly three-dimensional flow.

60 So, it is crucial to keep these factors in mind when discussing
 61 the current results. It is expected that including these important
 62 considerations will improve the computational estimations. The
 63 authors plan to continue their research in AFTRF, including these
 64 two factors in the near future. The current plan is to perform the

Table 4

Measured and computed percent change in C_{pt} at the ro-
 tor inlet plane.

| | Experiment Area-Av. | CFD Area-Av. | CFD Mass-Av. |
|------------|---------------------|--------------|--------------|
| D14 | -1.08 | 6.77 | 6.01 |
| F02linear | -7.95 | 1.62 | 2.10 |
| F03curved | 9.38 | 7.38 | 6.92 |
| F03linear | 14.10 | 3.37 | 3.37 |
| F04curved | 15.06 | 6.95 | 6.20 |
| FC02linear | -7.07 | 3.43 | 1.64 |
| FC03curved | 9.18 | 6.35 | 5.70 |
| FC03linear | 7.43 | 6.99 | 6.26 |
| FC04curved | 4.28 | 6.58 | 5.57 |

computations in the presence of a rotor in motion with rotor-vane
 80 interaction and the rim seal flow.

81 The secondary flow region in Fig. 14 is not as distinct at the
 82 rotor inlet plane as in Fig. 13. The endwall boundary layer loss
 83 and secondary flow loss are combined. However, the Flat Insert
 84 experimental distribution in Fig. 14.a shows that the secondary
 85 flow starts around 26% span. Based on this information, experi-
 86 mental measurement shows that D14 reduced the loss up to 44%.
 87 Nevertheless, below 15% span, it increases the loss. The CFD simu-
 88 lation predicts in the same trend, the secondary flow in D14 is less
 89 than that of the Flat Insert, and the loss is higher near the end-
 90 wall. This observation is in accordance with the discussion for the
 91 results at the NGV exit plane. Both the experimental and computa-
 92 tional assessments suggest that the secondary loss core is closer to
 93 the endwall. The secondary flow region is diffused along the vane
 94 pitch near the endwall.

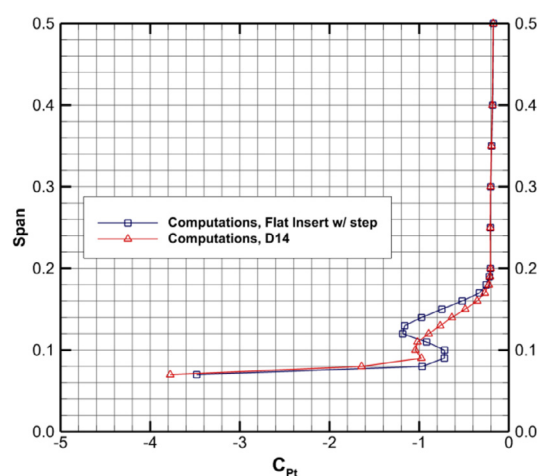
95 Table 4 lists the percent change in C_{pt} at the rotor inlet plane.
 96 Remember that the averaging is completed between 8% to 38%
 97 span for one pitch. Area-averaged experimental measurements tell
 98 that the most efficient designs are F03linear and F04curved with
 99 percent change values of 14.10 and 15.06, respectively. Besides,
 100 area-averaged percent change in CFD calculation for these designs
 101 are 3.37 for F03linear and 6.95 for F04curved. Based on the CFD
 102 area-averaged values, LE fillet designs combined with contoured
 103 endwall have the most total pressure loss reduction, except the
 104 short LE fillet configuration, FC02linear. The short LE fillet geome-
 105 tries, namely F02linear and FC02linear, increased C_{pt} in experimen-
 106 tal measurements. The experimental measurements for these cases
 107 confirm the numerical prediction.

108 The mass flow averaged C_{pt} is calculated at the NGV exit plane
 109 also, and the percent changes with respect to Flat Insert are listed
 110 in Table ???. Note that this mass flow averaging is obtained over the
 111 whole NGV passage exit. The most promising results come from
 112 FC03curved and FC03linear with percent change values of 1.84 and
 113 1.80, respectively.

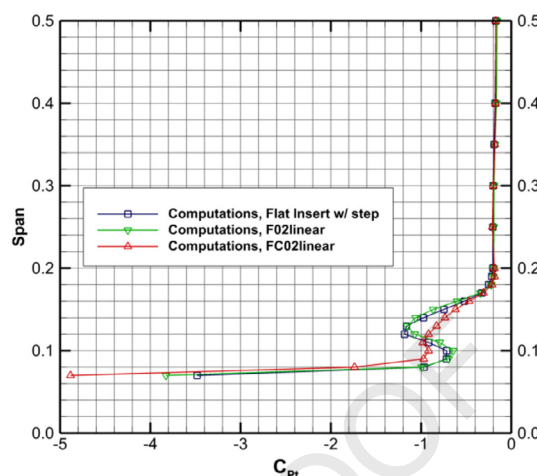
114 Fig. 14.g and Fig. 14.h depict the C_{pt} distribution for FC03curved
 115 and FC03linear, respectively. Both experimental measurements
 116 show that the secondary flow loss is reduced, without any in-
 117 crease in C_{pt} near 8% span. On the other hand, FC04curved, shown
 118 in Fig. 14.i, has a negative effect below 13% span. However, like
 119 the other designs, it decreased the secondary flow loss values. The
 120 numerical estimation of these three designs has a similar pattern,
 121 except below the secondary flow region. FC04curved has lowered
 122 the loss generation in the endwall boundary layer up to 11%.

6. Conclusions

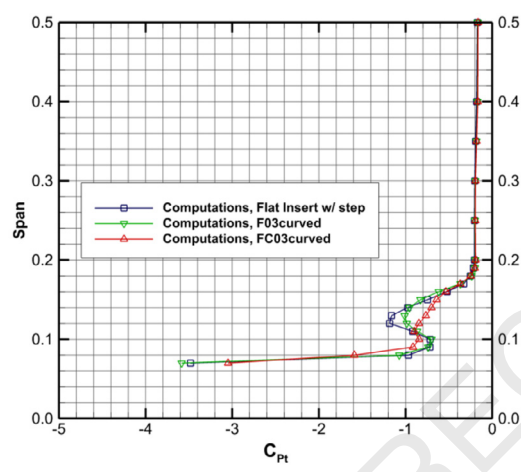
123 Four different LE fillets were designed for the NGV of the low-
 124 speed turbine rig, AFTRF. The aerodynamic performance of these
 125 LE fillets and a contoured endwall were tested experimentally and
 126 computationally. The fillets and endwall contouring surfaces were
 127 manufactured using an additive manufacturing technique (SLA).



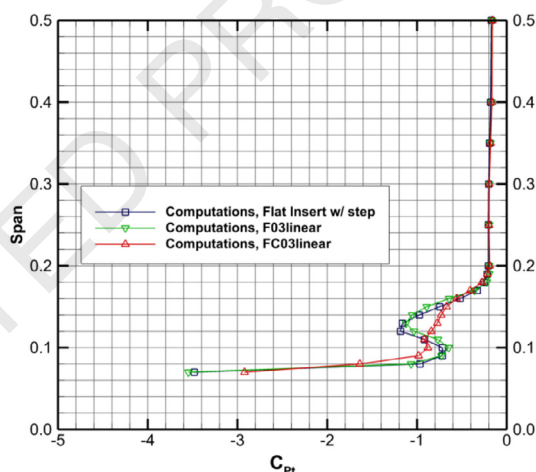
(a) D14



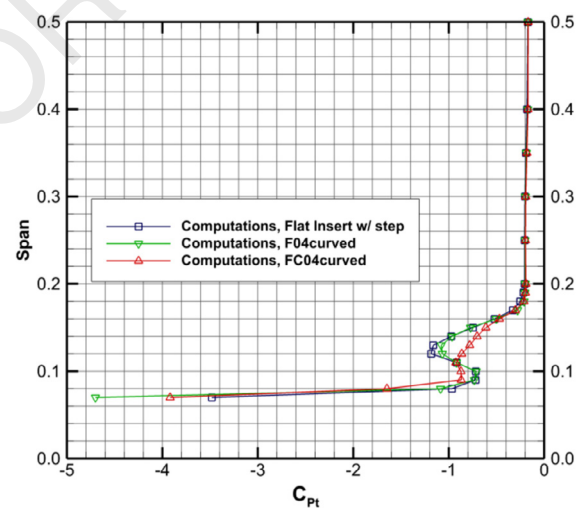
(b) F02linear and FC02linear



(c) F03curved and FC03curved



(d) F03linear and FC03linear



(e) F04curved and FC04curved

Fig. 13. Computational C_{Pt} distributions along the span at NCV exit plane. (C_{Pt} mass-averaged in the circumferential direction).

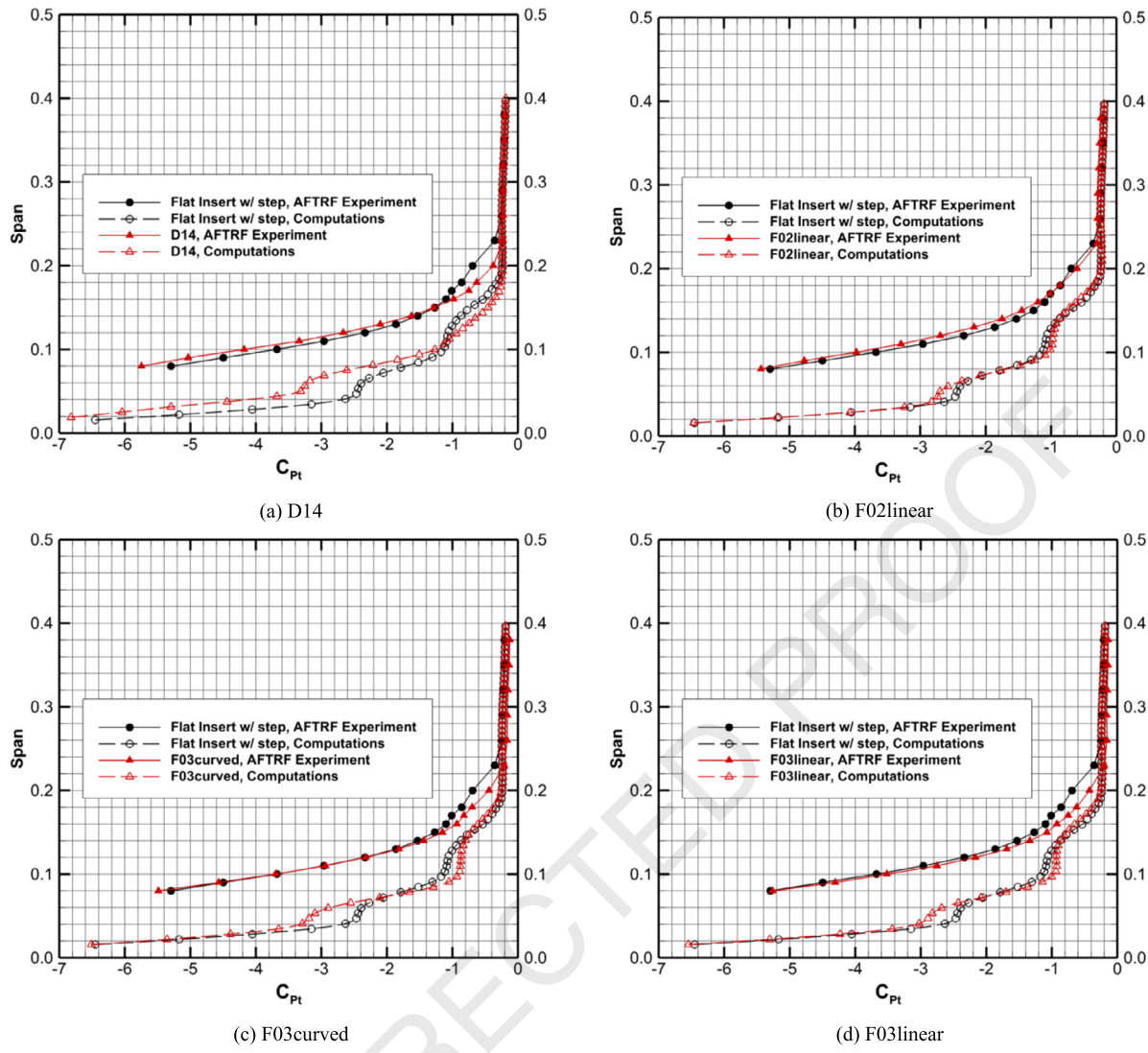


Fig. 14. Circumferentially area-averaged C_p distributions along the span at rotor inlet plane.

The numerical evaluation was initially achieved without the rotor simulation. A reference baseline, Flat Insert, with constant thickness and having a cylindrical surface was used. Two sets of LE fillets were manufactured using the SLA technique. The first set was attached to the Flat Insert, and the other set was sitting on the contoured endwall, D14.

The Flat Insert, located in the NGV passage, extended from one midspan chord upstream of LE downstream of TE where the NGV row ended. Therefore, it had a backward-facing step. To distinguish this step's flow influence, a computational assessment study was conducted with and without a backward-facing step. The comparison showed that the C_p distribution is 1% closer to the endwall in the case with the backward-facing step. The loss is diffused after the step.

LE fillets managed to remove the horseshoe vortex occurring in front of the LE. In one of the LE fillet cases sitting on Flat Insert, the CFD results at the NGV exit showed that the mass-averaged loss value was reduced by 1.31% for the whole passage exit. One of the LE fillets increased the loss at the NGV exit. At the rotor inlet plane, the experimental measurements were taken between 8% and 38% span. The area-averaged loss values showed a different trend. The most efficient one turned out to increase the loss after the backward step. The other three designs decreased the area-

averaged loss with a maximum reduction of 15.06%. CFD estimated that all designs reduced the area-averaged C_p up to 7.38%.

The contoured endwall effectively weakened the secondary flow region. Mass-averaged loss before the step at the NGV exit was reduced by 0.31%. However, area-averaged experimental measurement showed that it increased the loss at the rotor inlet plane, although CFD calculated a 6.77% decrease.

The combination of contoured endwall and LE fillets were also tested. Before the step, three of the designs worked well, and the loss was estimated less than Flat Insert, up to 1.84%. The rotor inlet plane experiments confirmed this estimation. The same design had a 9.18% reduction in area-averaged loss, whereas the CFD at this plane calculated a 6.35% reduction.

The current study shows that not all of the present CFD evaluations are in accordance with the experimental measurements. The authors attribute this to two reasons. One of them is the rotor-vane interaction that is not included in the current simulations. The computations are carried on without the rotor. Only the NGV passage flow is simulated. The second reason is excluding the rim seal flow entering into the rotating blade passages from the simulations. The authors plan to present their research in the AFTRF soon, including the presence of the rotor in motion with rotor-vane interaction and the rim seal flow.

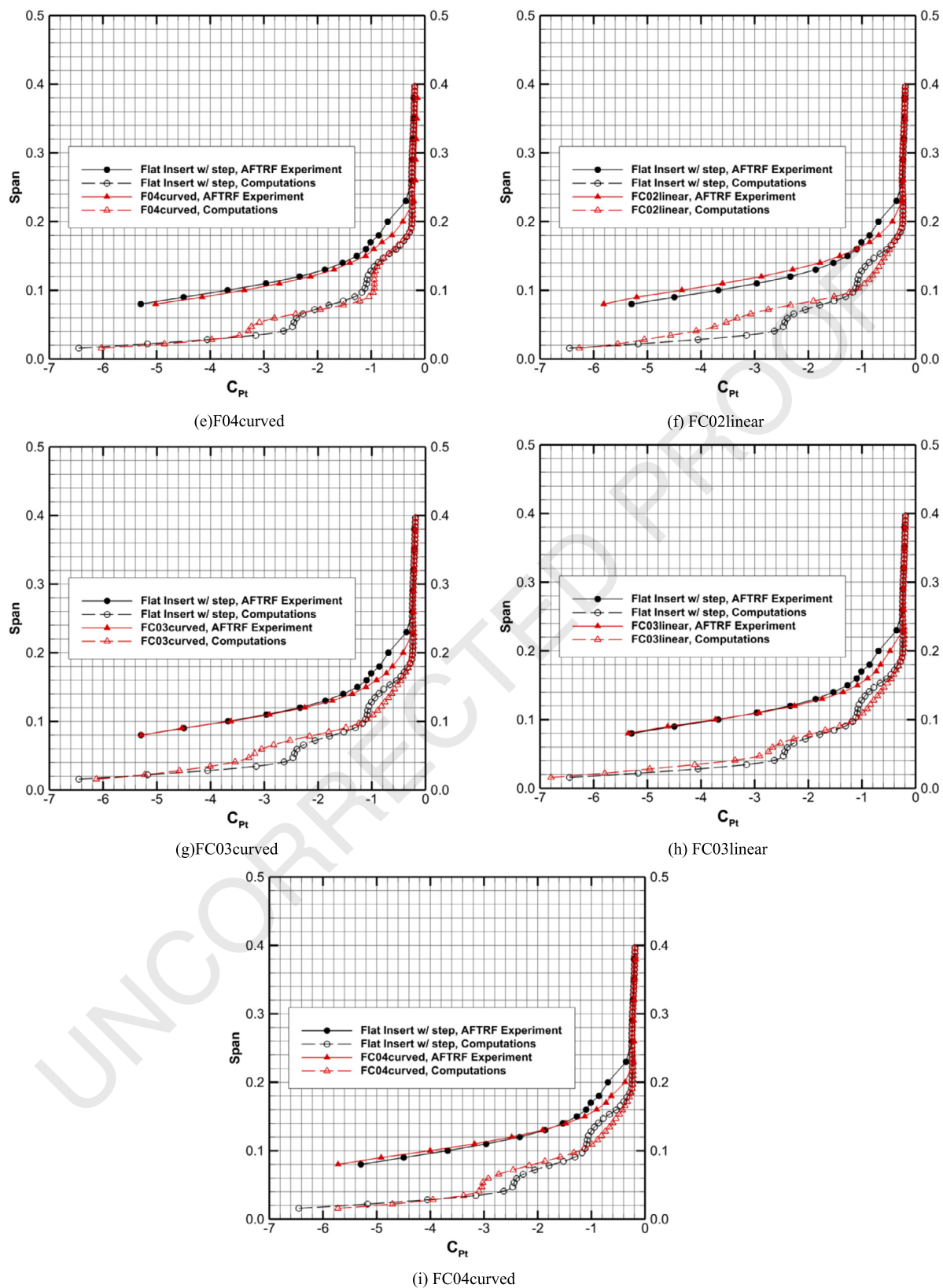


Fig. 14. (continued)

1 Declaration of competing interest

2 The authors declare that they have no known competing financial interests or personal relationships that could have appeared to influence the work reported in this paper.

7 Acknowledgements

9 The authors acknowledge the financial support provided by
 10 Siemens Energy Inc., Orlando. They thank Dr. Matthew Mont-
 11 gomery, Dr. Prakash Chander, Dr. Michael Crawford, Andrew Lo-
 12 haus, Anthony Malandra, Ching-Pang Lee, Boris Dobrzynski, Hum-
 13 berto Zuniga, Ken Landis, and Dirk Nuernberger. The authors are
 14 thankful to Dr. Ali Akturk for his support during this study. This
 15 paper's experimental and computational results were initially pre-
 16 sented at an ASME conference in Copenhagen, Denmark (GT2012-
 17 69304). Permission from the ASME Publications Department was
 18 granted to publish an extended version of this material in a non-
 19 ASME Journal. The authors are also indebted to Dr. Peter R. Eisen-
 20 man of Program Development Company, LLC for his great help in
 21 grid development for our study. M. Catalano and K. Heller were
 22 extremely helpful in high-performance-computing support during
 23 the study.

25 References

- [1] O.P. Sharma, T.L. Butler, Predictions of endwall losses and secondary flows in axial flow turbine cascades, *J. Turbomach.* 109 (2) (1987) 229–236, <https://doi.org/10.1115/1.3262089>.
- [2] J.D. Denton, Loss mechanisms in turbomachines, *J. Turbomach.* 115 (4) (1993) 621–650, <https://doi.org/10.1115/1.2929299>.
- [3] H. Sauer, R. Müller, K. Vogeler, Reduction of secondary flow losses in turbine cascades by leading edge modifications at the endwall, *J. Turbomach.* 123 (2) (2001) 207–213, <https://doi.org/10.1115/1.1354142>.
- [4] G.A. Zess, K. Thole, Computational design and experimental evaluation of using a leading edge fillet on a gas turbine vane, *J. Turbomach.* 124 (2) (2002) 167–175, <https://doi.org/10.1115/1.1460914>.
- [5] T.I.-P. Shih, Y.-L. Lin, Controlling secondary-flow structure by leading-edge airfoil fillet and inlet swirl to reduce aerodynamic loss and surface heat transfer, *J. Turbomach.* 125 (1) (2003) 48–56, <https://doi.org/10.1115/1.1518503>.
- [6] A.T. Lethander, K.A. Thole, G. Zess, J. Wagner, Vane-endwall junction optimization to reduce turbine vane passage adiabatic wall temperatures, *J. Propuls. Power* 20 (6) (2004) 1105–1116, <https://doi.org/10.2514/1.3887>.
- [7] S. Becz, M.S. Majewski, L.S. Langston, Leading edge modification effects on turbine cascade endwall loss, in: ASME Turbo Expo 2003, GT2003-38898, Atlanta, U.S.A., 2003.
- [8] S. Becz, M.S. Majewski, L.S. Langston, An experimental investigation of contoured leading edges for secondary flow loss reduction, in: SME Turbo Expo 2004, ASME Paper No. GT2004-53964, Vienna, Austria, 2004.
- [9] G.I. Mahmood, R. Gustafson, S. Acharya, Experimental investigation of flow structure and Nusselt number in a low-speed linear blade passage with and without leading-edge fillets, *J. Heat Transf.* 127 (5) (2005) 499–512, <https://doi.org/10.1115/1.1865218>.
- [10] C. Hu, H. Liu, K. Geng, R. Rong, Numerical investigation and loss estimation of high-pressure turbine cascade flow with contoured endwall and incoming wakes, *Aerosp. Sci. Technol.* 107 (106335) (2020), <https://doi.org/10.1016/j.ast.2020.106335>.
- [11] K.N. Kiran, S. Anish, An investigation on the effect of pitchwise endwall design in a turbine cascade at different incidence angles, *Aerosp. Sci. Technol.* (ISSN 1270-9638) 71 (2017) 382–391, <https://doi.org/10.1016/j.ast.2017.09.032>.
- [12] S. Han, R.J. Goldstein, Influence of blade leading edge geometry on turbine endwall heat (mass) transfer, *J. Turbomach.* 128 (4) (2005) 798–813, <https://doi.org/10.1115/1.2221326>.
- [13] K. Ananthakrishnan, M. Govardhan, Influence of fillet shapes on secondary flow field in a transonic axial flow turbine stage, *Aerosp. Sci. Technol.* (ISSN 1270-9638) 82–83 (2018) 425–437.
- [14] Ö.H. Turgut, C. Camci, A nonaxisymmetric endwall design methodology for turbine nozzle guide vanes and its computational fluid dynamics evaluation, in: ASME 2011 International Mechanical Engineering Congress and Exposition, IMECE2011-64362, Colorado, U.S.A., 2011, pp. 37–49.
- [15] N.W. Harvey, M.G. Rose, M.D. Taylor, S. Shahpar, J.C. Hartland, D.G. Gregory-Smith, Nonaxisymmetric turbine end wall design: part I—three-dimensional linear design system, *J. Turbomach.* 122 (2) (2000) 278–285, <https://doi.org/10.1115/1.555445>.
- [16] J.C. Hartland, D.G. Gregory-Smith, N.W. Harvey, M.G. Rose, Nonaxisymmetric turbine end wall design: part II—experimental validation, *J. Turbomach.* 122 (2) (2000) 286–293, <https://doi.org/10.1115/1.555446>.
- [17] N.W. Harvey, G. Brennan, D.A. Newman, M.G. Rose, Improving turbine efficiency using non-axisymmetric end walls: validation in the multi-row environment and with low aspect ratio blading, in: ASME Turbo Expo 2002: Power for Land, Sea, and Air, vol. 5, ASME GT2002-30337, Amsterdam, The Netherlands, 2002.
- [18] T. Sonoda, M. Hasenjäger, T. Arima, B. Sendhoff, Effect of end wall contouring on performance of ultra-low aspect ratio transonic turbine inlet guide vanes, *J. Turbomach.* 131 (1) (2009) 011020, <https://doi.org/10.1115/1.2813015>.
- [19] A. Rehman, B. Liu, Numerical investigation and non-axisymmetric endwall profiling of a turbine stage, *J. Therm. Sci.* 28 (2019) 811–825, <https://doi.org/10.1007/s11630-019-1154-0>.
- [20] M. Zaccaria, B. Lakshminarayana, Investigation of three-dimensional flowfield at the exit of a turbine nozzle, *J. Propuls. Power* 11 (1) (1995) 55–63, <https://doi.org/10.2514/3.23840>.
- [21] B. Lakshminarayana, C. Camci, I. Halliwell, M.A. Zaccaria, Design and development of a turbine research facility to study rotor-stator interaction effects, *Int. J. Turbo Jet-Engines* 13 (1996) 155–172, <https://doi.org/10.1515/TJJ.1996.13.1.155>.
- [22] C. Camci, Experimental and Computational Methodology for Turbine Tip Desensitization, Von Karman Institute for Fluid Dynamics Lecture Series, Brussels, Belgium, ISBN 2-930389-51-6, 2004.
- [23] M.A. Zaccaria, An Experimental Investigation into the Steady and Unsteady Flow Field in an Axial Flow Turbine, Ph.D. Thesis, The Pennsylvania State University, University Park, PA, 1994.
- [24] <http://www.unitedsensorcorp.com/kiel.html>, United Sensor Corporation [Online].
- [25] Ö.H. Turgut, C. Camci, A nonaxisymmetric endwall design approach and its computational assessment in the NGV of an HP turbine stage, *Aerosp. Sci. Technol.* 47 (September December 2015) 456–466, <https://doi.org/10.1016/j.ast.2015.09.014>.
- [26] Z. Tao, B. Yu, Y. Li, L. Song, J. Li, Effects of non-axisymmetric endwall contouring on aerothermal performance of a gas turbine blade endwall with a purge flow, *Int. J. Therm. Sci.* (ISSN 1290-0729) 164 (2021) 106921, <https://doi.org/10.1016/j.ijthermalsci.2021.106921>.
- [27] P. Chen, K. Zhao, X. Li, J. Ren, H. Jiang, Effects of varying non-axisymmetric contours of the turbine endwall on aerodynamics and heat transfer aspects: a sensitivity analysis study, *Int. J. Therm. Sci.* (ISSN 1290-0729) 161 (ISSN) (2021) 106689.
- [28] L.S. Langston, Secondary flows in axial turbines - a review, in: *Heat Transfer in Gas Turbine Systems*, Ann. N.Y. Acad. Sci. (ISSN 0077-8923) 934 (2001) 11–26.
- [29] C.-H. Sung, C.-W. Lin, Numerical investigation on the effect of fairing on the vortex flows around airfoil/flat-plate junctures, in: AIAA 26th Aerospace Sciences Meeting, Reno, NV, 1988.
- [30] F.R. Menter, Two-equation eddy-viscosity turbulence models for engineering applications, *AIAA J.* 32 (8) (1994) 1598–1605, <https://doi.org/10.2514/3.12149>.
- [31] Ö.H. Turgut, C. Camci, A computational validation of turbine nozzle guide vane aerodynamic experiments in an HP turbine stage, in: ASME 2011 International Mechanical Engineering Congress and Exposition, ASME Paper No. IMECE2011-64352, Denver, Colorado, U.S.A., 2011, pp. 23–35.
- [32] Ö.H. Turgut, C. Camci, Factors influencing computational predictability of aerodynamic losses in a turbine nozzle guide vane flow, *J. Fluids Eng.* 138 (5) (May 2016) 051103, <https://doi.org/10.1115/1.4031879>.
- [33] J.Y. Kim, A.J. Ghajar, C. Tang, G.L. Foutch, Comparison of near-wall treatment methods for high Reynolds number backward-facing step flow, *Int. J. Comput. Fluid Dyn.* 19 (7) (2005) 493–500, <https://doi.org/10.1080/10618560500502519>.